Mesoscopic architectures of porous coordination polymers fabricated by pseudomorphic replication

AUTHOR(S):

Reboul, Julien; Furukawa, Shuhei; Horike, Nao; Tsotsalas, Manuel; Hirai, Kenji; Uehara, Hiromitsu; Kondo, Mio; Louvain, Nicolas; Sakata, Osami; Kitagawa, Susumu

CITATION:

Reboul, Julien ...[et al]. Mesoscopic architectures of porous coordination polymers fabricated by pseudomorphic replication. Nature materials 2012, 11(8): 717-723

ISSUE DATE:

2012-06-24

URL:

http://hdl.handle.net/2433/158311

Mesoscopic architectures of porous coordination polymers fabricated by pseudomorphic replication

Julien Reboul[1,2], Shuhei Furukawa[1,2]*, Nao Horike[2], Manuel Tsotsalas[1,2], Kenji Hirai[3], Hiromitsu Uehara[2], Mio Kondo[1,2], Nicolas Louvain[1,2], Osami Sakata[4], and Susumu Kitagawa[1,2,3]*

[1]Institute for Integrated Cell-Material Sciences (WPI-iCeMS), Kyoto University, Yoshida, Sakyo-ku, Kyoto 606-8501, Japan

[2]ERATO Kitagawa Integrated Pores Project, Japan Science and Technology Agency (JST), Kyoto Research Park Bldg #3, Shimogyo-ku, Kyoto 600-8815, Japan

[3]Department of Synthetic Chemistry and Biological Chemistry, Graduate School of Engineering, Kyoto University, Katsura, Nishikyo-ku, Kyoto 615-8510, Japan

[4]Synchrotron X-ray Station at SPring-8, National Institute for Materials Science, Kouto, Sayo, Hyogo 679-5198, Japan

* To whom correspondence should be addressed: shuhei.furukawa@icems.kyoto-u.ac.jp (S.F.), kitagawa@sbchem.kyoto-u.ac.jp (S.K.)

The spatial organisation of porous coordination polymer (PCP) crystals into higher-order structures is critical for their integration into separation systems, heterogeneous catalysts, ion/electron transport and photonic devices. Here, we demonstrate a rapid method to spatially control the nucleation site, leading to the formation of mesoscopic architecture in PCPs, in both two and three dimensions. Inspired by geological processes, this method relies on the morphological replacement of a shaped sacrificial metal oxide used both as a metal source and as an "architecture-directing agent" by an analogous PCP architecture. Spatiotemporal harmonisation of the metal oxide dissolution and the PCP crystallisation allowed for preservation of very fine mineral morphological details of periodic alumina inverse opal structures. The replication of randomly structured alumina aerogels resulted in a PCP architecture with hierarchical porosity in which the hydrophobic micropores of the PCP and the mesopores/macropores inherited from the parent aerogels synergistically enhanced the material's selectivity and mass transfer for water/ethanol separation.

Pseudomorphic mineral replacement events consist in the transformation of a mineral phase that is out of equilibrium into a more thermodynamically stable phase, involving dissolution and reprecipitation sub-processes.[1] This natural phenomenon is characterised by the preservation of the shape and dimensions of the replaced parent phase whenever the kinetics of its dissolution are coupled with the kinetics of nucleation and crystallisation of the new phase. The initiation and spatiotemporal harmonisation of these re-equilibration reactions rely on parameters that are controllable in the laboratory. Therefore, the application of this natural process using pre-shaped sacrificial supports is an attractive strategy for introducing structural hierarchy and hence for improving the range of properties of various functional materials.[2,3] However, although the pseudomorphic replacement process is responsible for the generation of a variety of mineral phases in natural environments, this phenomenon has so far been rarely used as a strategy for the synthesis of functional materials and its application was limited to the production of purely mineral materials, for instance, complex metal sulfides,[4] hydroxyapatites[5] and zeolites.[6,7]

Porous coordination polymers (PCPs), constructed via the assembly of metal centres with organic linkers, are an intriguing class of crystalline microporous materials.[8-13] While PCPs demonstrate a range of properties that make them ideal for applications in gas storage,[14] catalysis,[15,16] sensing,[17] proton-conduction[18] and adsorptive separation,[19] their utilisation in practical applications is limited due to the poor processability of PCPs that are produced as bulk powders or single crystals through homogeneous crystallisation. The increasing number of reports that focus on the processing of PCPs into thin films,[20] two-dimensional patterns[21] and spheres[22] accounts for the significance of their integration into directly applicable materials. Control of the crystallisation processes is traditionally performed on substrates by the induction of heterogeneous nucleation[23,24] or by the direct deposition[25,26] of PCP crystals. However, the limitations of these techniques, in terms of the lack of control over the spatial localisation of the heterogeneous crystallisation, hinder the construction of designable higher-order architectures. Here, we demonstrate a coordination replication method by applying the pseudomorphic replacement process to introduce organic elements into a pre-shaped dense metal oxide phase. This process leads to the

simultaneous formation of coordination complexes at the molecular scale and to the construction of a mesoscopic PCP architecture by replicating the parent metal oxide phase (Fig. 1).

Because of its ubiquitous nature, processability and well-studied dissolution behaviour in the presence of organic acid molecules in natural environments (chemical weathering),[27] the alumina phase was selected as metal reservoir and mesoscale architecture-directing agent.[28] A two-dimensional honeycomb pattern and a three-dimensional inverse opal structure were first constructed as model parent architectures to emphasise the potential of our strategy in terms of the construction of a mesoscopic PCP architecture. By taking advantage of the unique characteristic of PCPs, whereby a suitable choice of both metal ions and organic ligands allows for a tailored pore size, pore surface functionality and framework flexibility, we constructed mesoscopic PCP architectures with different pore characteristics. We also showed the potential use of this strategy for the preparation of materials with enhanced functionality compared with conventional powders. After coordination replication, the selection of both

1,4-naphthalenedicarboxylic acid (H_2ndc) as an organic ligand and a randomly structured alumina aerogel as the parent architecture led to the formation of a hierarchical, porous system constructed from highly hydrophobic PCP crystals with efficient mass transport properties for water/ethanol vapour-phase separation.

Assemblies of 1 μm polystyrene (Ps) beads were used as hard templates for the synthesis of two-dimensional honeycomb patterns or three-dimensional inverse opal structures[29] (Fig. 2). After the reaction of the pattern at 180°C for 10 min in an aqueous solution of H_2ndc under microwave conditions, synchrotron X-ray diffraction measurements unambiguously confirmed the formation of an aluminium naphthalene dicarboxylate framework[30] $[Al(OH)(ndc)]_n$ based on one-dimensional inorganic chains of $[Al(OH)(COO)_2]_n$ (Figs. 2a-c). Characterisation by field-emission scanning electron microscopy (FESEM) showed that the two-dimensional alumina patterns were composed of well-ordered hexagonal arrangements of macro-voids and alumina walls approximately 50-nm thick (Fig. 2d). After the reaction, FESEM revealed that a perfect PCP replica of the

alumina pattern was obtained (Fig. 2e). Intergrown PCP crystals of 10 to 200 nm with a nearly cubic shape replaced the 50-nm-thick alumina walls.

The coordination replication of a three-dimensional alumina inverse opal structure (Fig. 2f) led to the formation of a PCP-based material with a hierarchical porosity (Figs. 2g and 2h), combining the microporosity of the PCP and the macroporosity of the inverse opal structure. The PCP replica exhibited macropores with a diameter of 800 nm connected by windows of 100 to 200 nm in width (Fig. 2g). Similar to the two-dimensional hexagonal pattern, the walls of the PCP macroporous materials were composed of well-intergrown crystals ranging from 10 to 200 nm in size.

The PCP product inherits a shape that is identical to that of the alumina parent architecture. Careful observation of the FESEM images revealed that even the fine morphological details of the parent product were preserved after transformation into the PCP crystals (Supplementary Figs. S1 and S2). Such preservation strongly suggests a coupled “dissolution-reprecipitation” mechanism,[1] in which the metastable parent product dissolves in the fluid at the solid-liquid interface and immediately crystallises as a new

stable daughter phase at the same site as the dissolved precursor. This mechanism was confirmed via an FESEM analysis obtained from time course experiments with the reaction at 140°C (Fig. 3). After a 1 s reaction time, the smooth surfaces of the alumina pattern (Fig. 3a) became rougher (Fig. 3b) due to the coating of small ill-defined nuclei with lengths of approximately 10 nm. From 4 s to 10 s (Figs. 3c-e), the number of crystals with a size between 10 and 100 nm increased. Simultaneously, the reaction front at the interface between the alumina and the PCP crystal progressively disappeared with time, providing evidence of alumina consumption to form the PCP crystals (Fig. 3e). As shown in Figures 3d-g, the crystals were not connected to each other, and voids of a few nanometres were clearly visible between them. The presence of porosity within the new material formed is a classic feature of the coupled dissolution-reprecipitation mechanism.[1,31] After a reaction time of 60 s, the PCP replica of the alumina parent pattern, composed of densely packed crystals, was finally formed (Fig. 3h). Based on these observations, the mechanism of pseudomorphic mineral replacement reactions can hence be adapted to our coordination replication process, as shown in Figure 4 and Supplementary Figure S3.

The coordination replication was then applied with two other dicarboxylic acids (Supplementary Fig. S4-7). A three-dimensional alumina inverse opal crystal architecture composed of inter-grown octahedral $\{[Al_3O(OH)(H_2O)_2](btc)_2\}_n$ crystals,[32] also known as MIL-100, was synthesised via the replication of the analogous alumina architecture in a solution of benzene tricarboxylic acid (H_2btc), used as an organic ligand (Supplementary Figs. S4 and S5). Instead, the use of benzene dicarboxylic acid (H_2bdc) led to the formation of a PCP replica of the inverse opal structure based on an assembly of $[Al(OH)(bdc)]_n$ crystals[33] (known as MIL-53) with a plate-like morphology (Supplementary Figs. S6 and S7). Hence, the utilisation of three different organic ligands resulted in the construction of a three-dimensional PCP architecture, presenting three remarkable porous properties based on the stiff and hydrophobic $[Al(OH)(ndc)]_n$ framework, the mesoporous $\{[Al_3O(OH)(H_2O)_2](btc)_2\}_n$ framework and the $[Al(OH)(bdc)]_n$ framework that is well-known for its flexible behaviour under hydration/dehydration.

Here, we focused on the hydrophobic micropores of $[Al(OH)(ndc)]_n$ to implement a new water/ethanol separation system. Extraction of bioethanol from its aqueous synthesis

media is important for the development of the next generation of fuel systems.[34] However, suitable porous materials that combine a high selectivity for ethanol against water with a high adsorption capacity are still rare, and such separation has never been performed by molecule-based porous materials. The selective vapour adsorption of $[Al(OH)(ndc)]_n$ for ethanol versus water was confirmed by a single-component adsorption isotherm obtained at 298 K (Supplementary Fig. S8). After packing the powders of $[Al(OH)(ndc)]_n$ crystals into a glass tube, we demonstrated for the first time the water/ethanol separation capacity of PCPs by means of a binary vapour-phase breakthrough experiment for an equimolar mixture of water/ethanol with a separation selectivity of 2.26 (Supplementary Fig. S9). However, when integrated into the chemical engineering processes, the dimensions of the equipment, the attainable product recovery and the resulting power consumption are tightly linked to the macroscopic architecture of the microporous material, which affects decisive parameters such as the mass transfer properties and the pressure drop.[35]

We explored the prospective application of the coordination replication method by the inclusion of $[Al(OH)(ndc)]_n$ crystals as an integral part of an architectural design

containing a multimodal porosity. To maximise the adsorption area, mechanical strength and flow and transport through the structure of the mesoscopic PCP architectures, the highly open and disordered alumina networks of two aerogels with distinct pore properties were chosen as parent structures.[36] As indicated by nitrogen sorption measurements (Supplementary Figs. S10-12) and FESEM (Supplementary Figs. S13 and S14), one aerogel contains an intrinsic mesoporosity with a median mesopore size of 94 nm, and the other one is a hierarchically porous aerogel composed of both mesopores (38 nm) and macropores (1 μm).[37] After replication of the parent structures, two mesoscopic PCP architectures with two types of hierarchical porosity were obtained (Fig. 5 and Supplementary Fig. S15). Replication of the mesoporous alumina aerogel results in the formation of the microporous/mesoporous PCP architecture called **Meso-PCP**. Replication of the mesoporous/macroporous alumina aerogel results in the microporous/mesoporous/macroporous PCP architecture called **Macro-PCP**.

The entire architectures of **Meso-PCP** and **Macro-PCP** are unambiguously composed of thoroughly intergrown crystals of $[Al(OH)(ndc)]_n$ (Figs. 5b and 5c and

Supplementary Figs. S16-S18). As shown by the nitrogen sorption measurements (Supplementary Figs. S10 and S11), the characteristic mesopores of the parent aerogels were maintained even after replication into the corresponding mesoscopic PCP architectures of **Meso-PCP** and **Macro-PCP**, which additionally possess microporosity based on the framework $[Al(OH)(ndc)]_n$ structure. The formation of the PCP microporosity was confirmed with a carbon dioxide sorption isotherm (Supplementary Figs. S19), in which a significant increase of adsorption at a low relative pressure, ranging from 0 to 0.1, was observed after replication (Supplementary Figs. S20). Note that the unique Type 1 sorption profile and the saturation capacity (up to 143 $cm^3(STP)\cdot g^{-1}$) of the mesoscopic PCP architectures are comparable to those of the $[Al(OH)(ndc)]_n$ powders synthesised from the aluminium salt, as reported in the literature (138 $cm^3(STP)\cdot g^{-1}$).

Breakthrough experiments performed with **Meso-PCP** or **Macro-PCP** for the separation of an equimolar binary water/ethanol mixture demonstrated the effect of the adsorbent architecture over the separation efficiency (Fig. 6). Importantly, the shape, size (Supplementary Fig. S21), crystallinity (Supplementary Figure S18) and microporosity

(Supplementary Figure S19) of PCP crystals that construct both **Meso-PCP** and **Macro-PCP** were shown to be analogous. An equal bed voidage was guaranteed by packing columns with pieces of **Meso-PCP** and **Macro-PCP** of the same size (approximately 200 μm, Supplementary Fig. S22). Also, the weights of packed materials and the procedures applied for packing **Meso-PCP** and **Macro-PCP** into the glass tubes were rigorously identical. Therefore, difference in separation efficiency observed between **Meso-PCP** and **Macro-PCP** in the following section can be exclusively explained by their distinct mesoscopic architectures. In contrast with the parent alumina aerogel (Supplementary Fig. S23), both mesoscopic PCP architectures enabled a significant water/ethanol separation with a separation selectivity[38] of 2.56 for **Meso-PCP** and 1.84 for **Macro-PCP**. Importantly, we observed a reduction in the breakthrough time and lower pressures at the inlet of the column with **Meso-PCP** and **Macro-PCP** compared with the powder samples (inlet pressure = 54, 33 and 256 kPa; water breakthrough time = 12.1, 8.6 and 15 min; ethanol breakthrough time = 24, 14.5 and 40 min for **Meso-PCP**, **Macro-PCP** and the powder, respectively). In addition, steeper breakthrough fronts were observed when

the separation process was performed with **Meso-PCP** and **Macro-PCP** compared with the powder, indicating more uniform water and ethanol vapour-phase velocities through the column. These results show the beneficial effect of the mesoporosity and macroporosity of the PCP architecture on the performance of the separation column, which provide short diffusion paths towards the adsorption sites located within the microporosity of the PCP crystals.

We also observed a significant difference between **Meso-PCP** and **Macro-PCP** for the separation performance. As a consequence of the macroporosity, the use of **Macro-PCP** led to a lower separation time and a lower pressure at the inlet than that of **Meso-PCP**. In contrast, the smaller pore size of **Meso-PCP** and the higher exposed surface area of PCP within this architecture (Supplementary Fig. S12) allowed for higher ethanol retention and improved separation selectivity. The loss of adsorbent loading observed with **Macro-PCP** due to its large diffusion paths can be avoided by the design of the mesoscopic PCP architecture.

These results demonstrate a new method for designing mesoscopic architecture

based on PCP crystals in two and three dimensions using a reliable and extremely fast coordination replication protocol. The kinetics and spatial coupling between the dissolution of a metastable alumina phase and the crystallisation of aluminium-based PCPs enables the production of both periodic and random mesoscopic PCP architectures through a pseudomorphic replacement mechanism. Assisted by the well-established processing of metal oxide, the precise localisation of parent metal oxide phases should permit the design of PCP architectures with a great variety of useful geometries. We believe that the construction of mesoscopic PCP architectures, achieved here through the conversion of an alumina phase into PCPs, can be extended to other metal oxide phases, such as iron oxide, zirconium oxide or nickel oxide, because the natural weathering processes of these metal oxides were studied[39,40] and because these mineral phases can be used for the formation of PCPs[41] once the condition of spatiotemporal coupling between dissolution and crystallisation is established.

Methods

Preparation of the two-dimensional hexagonal alumina patterns and three-dimensional alumina-based inverse opal structure. For preparation of the two-dimensional hexagonal patterns, a suspension of Ps beads with a diameter of 1 μm in ethanol was spread by spin coating (1000 rpm) on an amorphous silica plate previously treated for 24 h in a piranha solution. After drying for 10 h at room temperature, the colloidal film was annealed by a short thermal treatment of 1 min at 100°C and then placed for 3 h in a horizontally face-up configuration in a solution composed of 0.820 g of aluminium tri-sec-butoxide ($Al[OCH(CH_3)C_2H_5]_3$), 2.37 g of ethanol and 1.72 g of 60% nitric acid. After drying for 48 h at room temperature, the colloidal mask was calcined for 7 h at 580°C under nitrogen. The three-dimensional alumina-based inverse opal materials were obtained by the formation of multilayered colloidal crystal films on the silica plate at slow spinning rate (500 rpm).

Preparation of the two- and three-dimensional PCP-based replicates. Replication of the alumina pattern was performed with a microwave reactor (Initiator 2.5, Biotage). The

alumina pattern and inverse opal crystals on silica substrates (width = 0.5 cm, length = 1 cm) were placed in a 2 ml microwave container with 0.08 g 1,4-naphthalenedicarboxylic acid and 2 ml water. The microwave treatment was performed at 180°C for 10 min. The PCP-based replicate obtained was washed with water and dimethylformaldehyde. Time dependence experiments were performed at 140°C.

The comparative time dependence study with hydrothermal treatment was performed in 10 mL Teflon-lined autoclaves at 140°C for various times on samples, which were prepared using the same procedure.

For the application of the coordination replication with benzene tricarboxylic acid and benzene dicarboxylic acid, the inverse opal crystals on silica substrates (width = 0.5 cm, length = 1 cm) were placed in a 2 ml microwave container with 0.077 g benzenetricarboxylic acid or 0.061g of benzene dicarboxylic acid and 2 ml water. The microwave treatment was performed at 220°C for 10 s with the benzenetricarboxylic acid and 180°C for 3 min with the benzenedicarboxylic acid. The PCP-based replicates obtained were washed with dimethylformaldehyde, water and ethanol.

Preparation of the alumina aerogel. 649 mg of aluminum chloride hexahydrate ($AlCl_3.6H_2O$) were dissolved in a mixture of 0.6 ml of distilled H_2O and 0.740 ml of ethanol. Then, 0.560 ml of propylene oxide (PO) was added under ambient conditions (25°C). After being stirred for 1 min, the resultant homogeneous solution was kept for gelation and aging in an incubator at 40°C for 24h. The transparent solution turned into a translucent gel. After threefold solvent exchange with 2-propanol at 60°C for 24h, the wet gels were dried by a supercritical drying process in a SCLEAD-2BD autoclave from KISCO using supercritical carbon dioxide at 80°C and 14.0 MPa. The recovered aerogel preserved the dimensions of the corresponding wet gel.

Preparation of the alumina macroporous aerogel. The same procedure as for the synthesis of the mesoporous alumina aerogel was applied to obtain the macroporous alumina aerogel. 9 mg of poly(ethylene oxide) (PEO) was added to the 649 mg of aluminum chloride hexahydrate ($AlCl_3.6H_2O$) within the initial reagent mixture.

Preparation of the mesoscale PCP-based architectures (Meso-PCP and Macro-PCP). The alumina aerogel or the macroporous alumina aerogel was placed in a 2 ml microwave

container with 0.08 g of 1,4-naphthalenedicarboxylic acid and 2 ml water. The microwave treatment was performed at 180°C for 1 min. The PCP-based replicate obtained was washed with water and dimethylformaldehyde.

Preparation of the $[Al(OH)(ndc)]_n$ crystal powder. 375 mg of aluminum nitrate nonahydrate ($Al(NO_3)_3.6H_2O$) and 108 mg of 1,4-naphthalenedicarboxylic acid were mixed in 10 mL of water. A microwave treatment was performed at 180°C for 10 min. The white PCP powder obtained was washed with water and dimethylformaldehyde.

Breakthrough measurements in vapor phase. Breakthrough experiments in vapor phase for the equimolar water/ethanol gas mixture were performed using the experimental setup described in Supplementary Fig. S24. Briefly, 0.09 g of the $[Al(OH)(ndc)]_n$ PCP crystal powder or grinded **Meso-PCP** or grinded **Macro-PCP** were packed in a glass tube (L =5 cm; di = 3 mm). The adsorption column was then placed in an oven at 80°C and operated by introducing continuously an equimolar water/ethanol vapor mixture generated by BELFlow-3 from BEL JAPAN. The composition history of the mixtures collected at the outlet of the column was evaluated by a gas chromatographer GC-2014 from SHIMADZU

equipped with TPA 60-80/PEG 6000 columns. A thermal conductivity detector was connected to the GC column outlet. Peaks were identified by reference injections using series of different water or ethanol concentrations and by drawing calibration curves.

References:

1. Putnis, A. Mineral replacement reactions. *Rev. Miner. Geochem.* **70**, 87-124 (2009).

2. Antonietti, M. & Ozin, G. A. Promises and problems of mesoscale materials chemistry or why meso? *Chem. Eur. J.* **10**, 28-41 (2004).

3. Cölfen, H. & Mann, S. Higher-order organization by mesoscale self-assembly and transformation of hybrid nanostructures. *Angew. Chem. Int. Ed.* **42**, 2350-2365 (2003).

4. Xia, F. et al. Novel route to synthesize complex metal sulfides: hydrothermal coupled dissolution-reprecipitation replacement reactions. *Chem. Mater.* **20**, 2809-2817 (2008).

5. Roy, D. M. & Linneham, S. K. Hydroxyapatite formed from coral skeletal carbonate by hydrothermal exchange. *Nature* **247**, 220-222 (1974).

6. Anderson, M. W., Holmes, S. M., Hanif, N. & Cundy, C. S. Hierarchical pore structures through diatom zeolitization. *Angew. Chem. Int. Ed.* **39**, 2707-2710

(2000).

7. Xia, F. et al. Three-dimensional ordered arrays of zeolite nanocrystals with uniform size and orientation by a pseudomorphic coupled dissolution-reprecipitation replacement route. *Cryst. Growth Des.* **9**, 4902-4906 (2009).

8. Yaghi, O. M. et al. Reticular synthesis and the design of new materials. *Nature* **423**, 705-714 (2003).

9. Kitagawa, S., Kitaura, R. & Noro, S. Functional porous coordination polymers. *Angew. Chem. Int. Ed*. **43**, 2334-2375 (2004).

10. Férey, G. Hybrid porous solids: past, present, future. *Chem. Soc. Rev*. **37**, 191-214 (2008).

11. Dincã, M. & Long, J. R. Hydrogen Storage in Microporous Metal-Organic Frameworks with Exposed Metal Sites. *Angew. Chem. Int. Ed*. **47**, 6766-6779 (2008).

12. Blake, A. J. et al. Photoreactivity examined through incorporation in

metal-organic frameworks. *Nature Chem.* **2,** 688-694 (2010).

13. Farha, O. K. et al. De novo synthesis of a metal-organic framework material featuring ultrahigh surface area and gas storage capacities. *Nature Chem*. **2**. 944-948 (2010).

14. Zhao, X. et al. Hysteretic adsorption and desorption of hydrogen by nanoporous metal-organic frameworks. *Science.* **306**, 1012-1015 (2004).

15. Seo, J. S., et al. A homochiral metal-organic porous material for enantioselective separation and catalysis. *Nature* **404**, 982-986 (2000).

16. Kawamichi, T., Haneda, T., Kawano, M. & Fujita. M. X-ray observation of a transient hemiaminal trapped in a porous network. *Nature* **461,** 633-635 (2009).

17. Takashima, Y., et al. Molecular decoding using luminescence from an entangled porous framework. *Nature Commun* **2**, 168 (2011).

18. Hurd, J. A. et al. Anhydrous proton conduction at 150 ºC in a crystalline metal-organic framework. *Nature Chem*. **1**, 705-710 (2009).

19. Xiao, B. et al. Chemically blockable transformation and ultraselective

low-pressure gas adsorption in a non-porous metal organic framework. *Nature Chem.* **1**, 289-294 (2009).

20. Zacher, D., Shekhah, O., Wöll, C. & Fischer, R. A. Thin films of metal organic frameworks. *Chem. Soc. Rev.* **38**, 1418-1429 (2009).

21. Falcaro, P. et al. A new method to position and functionalize metal organic framework crystals. *Nature Commun*. **2**, 237 (2011).

22. Ameloot, R. et al. Interfacial synthesis of hollow metal-organic framework capsules demonstrating selective permeability. *Nature Chem*. **3**, 382-387 (2011).

23. Schoedel, A., Scherb, C. & Bein, T. Oriented nanoscale films of metal-organic frameworks by room-temperature gel-layer synthesis. *Angew. Chem. Int. Ed.* **49**, 7225-7228 (2010).

24. Wu, Y., et al. Metal-organic frameworks with a three-dimensional ordered macroporous structure: dynamic photonic materials. *Angew. Chem. Int. Ed.* **50**, 12518-12522 (2011).

25. Gascon, J., Aguado, S. & Kapteijn Manufacture of dense coatings of $Cu_3(BTC)_2$

(HKUST-1) on α-alumina. *Micropor. Mesopor. Mater.* **113**, 132-138 (2008).

26. Horcajada, P., et al. Colloidal route for preparing optical thin films of nanoporous metal-organic frameworks. *Adv. Mater.* **21**, 1931-1935 (2009).

27. Stumm, W. & Wollast, R. Coordination chemistry of weathering: kinetics of the surface-controlled dissolution of oxide minerals. *Rev. Geophys.* **28**, 53-69 (1990).

28. Masuda, H. & Fukuda, K. Ordered metal nanohole arrays made by a two-step replication of honeycomb structures of anodic alumina. *Science* **268**, 1466-1468 (1995).

29. Holland, B. T., Blanford, C. F. & Stein, A. Synthesis of macroporous minerals with highly ordered three-dimensional arrays of spheroidal voids. *Science.* **281**, 538-540 (1998).

30. Comotti, A., et al. Nannochannels of two distinct cross-sections in a porous Al-based coordination polymer. *J. Am. Chem. Soc.* **130**, 13664-13672 (2008).

31. Putnis, A. & Putnis, C.V. The mechanism of reequilibration of solids in the presence of a fluid phase. *J. Solid State Chem.* **180**, 1783-1786 (2007).

32. Volkringer, C., et al. Synthesis, single-crystal X-ray microdiffraction, and NMR characterizations of the giant pore metal-organic framework aluminium trimesate MIL-100. *Chem. Mater.* **21**, 5695-5697 (2009).

33. Loiseau, T., et al. A rationale for the large breathing of the porous aluminium terephtalate (MIL-53) upon hydration. *Chem. Eur. J.* **10**, 1373-1382 (2004).

34. Vane, M.L. Separation technologies for the recovery and dehydration of alcohols from fermentation broths. *Biofuels, Bioprod. Bioref.* **2**, 553-588 (2008).

35. Rezaei, F. & Webley, P. Structured adsorbents in gas separation processes. *Sep. Pur. Tech.* **70**, 243-256 (2010).

36. Rolison, D. R. Catalytic nanoarchitectures-the importance of nothing and the unimportance of periodicity. *Science* **299**, 1698-1701 (2003).

37. Tokudome, Y., et al. Structural characterization of hierarchically porous alumina aerogel and xerogel monoliths. *J. Colloid Interface Sci.* **338**, 506-513 (2009).

38. Bárcia, P.S., et al. Kinetic separation of hexane isomers by fixed-bed adsorption with a microporous metal-organic framework. *J. Phys. Chem. B.* **111**, 6101-6103

(2007).

39. Schwertmann, U. Solubility and dissolution of iron oxides. *Plant and Soil.* **130**, 1-25 (1991).

40. Ludwig, C., Casey, W.H. & Rock, P.A. Prediction of ligand-promoted dissolution rates from the reactivities of aqueous complexes. *Nature*, **375**, 44-47 (1995).

41. Guo, H., Zhu, G., Hewitt, I. J. & Qiu, S. “Twin Copper Source” growth of metal-organic framework membrane: $Cu_3(BTC)_2$ with high permeability and selectivity for recycling H_2. *J. Am. Chem. Soc.* **131**, 1646-1647 (2009).

Acknowledgements:

The authors thank Dr. Nobuhiro Morone, the support from CeMI, and Dr. Takaaki Tsuruoka for assistance with measurement for FESEM and Mr. Koichi Shiomi for assistance with breakthrough experiments. iCeMS is supported by World Premier International Research Initiative (WPI), MEXT, Japan.

Author Contributions:

S.F., J.R., and S.K. conceived and designed the experiments. J.R. N.H. and M.T. performed all synthetic and characterization experiments. S.F., K.H., H.U., M.K., N.L., and O.S. carried out synchrotron XRD measurements. J.R. carried out water/ethanol separation experiments. J.R. and S.F. analyzed the data and co-wrote the manuscript. All authors discussed the results and commented on the manuscript.

Competing Financial Interests:

The authors declare that they have no competing financial interests.

Figure Legends:

Figure 1. The coordination replication and mesoscopic architecture concept. The coordination replication method is based on the replacement of a metastable dense metal oxide phase (illustrated as a red honeycomb pattern) by more stable PCP crystals (as a blue honeycomb pattern). Local dissolution of the metal oxide phase provides the metal ions, which are immediately consumed by the formation of coordination frameworks with organic ligands (as yellow sticks) at metal oxide-solution interfaces. Therefore, morphological details are preserved. As the metal oxide is shaped in the first step using sol-gel process involving metal ions (depicted as red spheres), it acts not only as a metal source through its dissolution but also as an "architecture-directing agent". Here, the term "mesoscopic architecture" refers to architectural motifs hierarchically organised both at the macroscale (PCP crystalline architectures inherited from the parent metal oxide structure) and at the molecular scale (PCP frameworks composed of subunits organised at the molecular scale).

Figure 2. Coordination replication to form two- and three-dimensional mesoscopic architectures based on a porous aluminium coordination polymer. a. The crystal structure of the aluminium naphthalenedicarboxylate framework, $[Al(OH)(ndc)]_n$, reveals a three-dimensional framework composed of infinite chains of $Al(OH)_2O_4$ units connected with 1,4-naphthalenedicarboxylate ligands. **b.** A chain composed of corner-sharing octahedral $Al(OH)_2O_4$ units. **c**. Synchrotron X-ray diffraction pattern of the replica and the simulated pattern of $[Al(OH)(ndc)]_n$. **d.** Top-view FESEM images of the alumina hexagonal pattern. **e.** Top-view FESEM images of the aluminium PCP replica obtained after microwave treatment for 10 min at 180°C. **f.** Top-view FESEM image of the three-dimensional alumina inverse opal crystal before transformation. **g and h.** FESEM images of the PCP replica after transformation (top and side views, respectively). All scale bars = 1 μm.

Figure 3. Time-course monitoring of the coordination replication by FESEM. Images of (**a**) the alumina pattern and of the same sample after replication for (**b**) 1 s, (**c**) 4 s, (**d**) 6 s, (**e**) 10 s, (**f**) 20 s, (**g**) 40 s and (**h**) 60 s. All scale bars = 1 μm. This series of experiments was performed at 140°C, compared to 180°C for the sample shown in Fig. 2, because replication was completed at 180°C after 1 s, which made a time dependence study difficult. By performing the experiments at 140°C, the reaction was slowed down, allowing us to carefully follow the alumina transformation at different stages.

Figure 4. Schematic view of the coordination replication mechanism. We adapt the mechanism of pseudomorphic mineral replacement reactions that is well described in geochemistry to the coordination replication. **a**. Dissolution of alumina forms the interface layer supersaturated with respect to aluminium aqua complexes. A coordination reaction between dissolved aluminium cations and dicarboxylate ligands promotes the formation of PCP-nuclei composed of aluminium hydroxide oligomers connected with each other by the ligands. **b**. The PCP crystal grows from the crystal surfaces in contact with the supersaturated interface layer. As the alumina dissolves, the interface layer is enriched with freshly released aluminium cations that feed the crystal growth, together with the organic ligand. Alumina dissolution induces the creation of voids below the crystals, providing pathways for ligand diffusion from the solution to the reaction front. The crystal grows towards the alumina surface as indicated by the red arrow. Localisation of the supersaturated layer only at the interface between the alumina surface and the ligand solution is allowed by the fast crystallization kinetics compare to the alumina dissolution kinetics. Hence PCP crystal formation is maintained at the solid-liquid interface that

enables coordination replication. The crystal structure of Al-based PCP is simplified for clarity.

Figure 5. Replication of randomly structured alumina aerogels for the formation of mesoscopic PCP architectures used as water/ethanol separation systems. a. Schematic illustration of coordination replication from alumina aerogel and macroporous alumina aerogel parent structures to **Meso-PCP** and **Macro-PCP** analogous architectures, respectively. The different types of porosity composing the parent aerogels and the PCP-based replicas are indicated below each scheme. **b.** FESEM images of **Meso-PCP**. **c.** FESEM images of **Macro-PCP**. Scale bars = 10 µm for the main images. Scale bars = 1 µm for the images in inset.

Figure 6. Water/ethanol separation with the mesoscopic PCP architecture, Meso-PCP or Macro-PCP. Binary breakthrough separation profiles for the equimolar separation of mixture of ethanol (circle) /water (triangle) at T=80°C obtained with **Macro-PCP** (red), **Meso-PCP** (blue) and powders (black). Compared to the PCP powder, mesoscale architectures enhance the mass transfer kinetics, resulting in lower breakthrough times of water and ethanol while keeping significant separation efficiency.

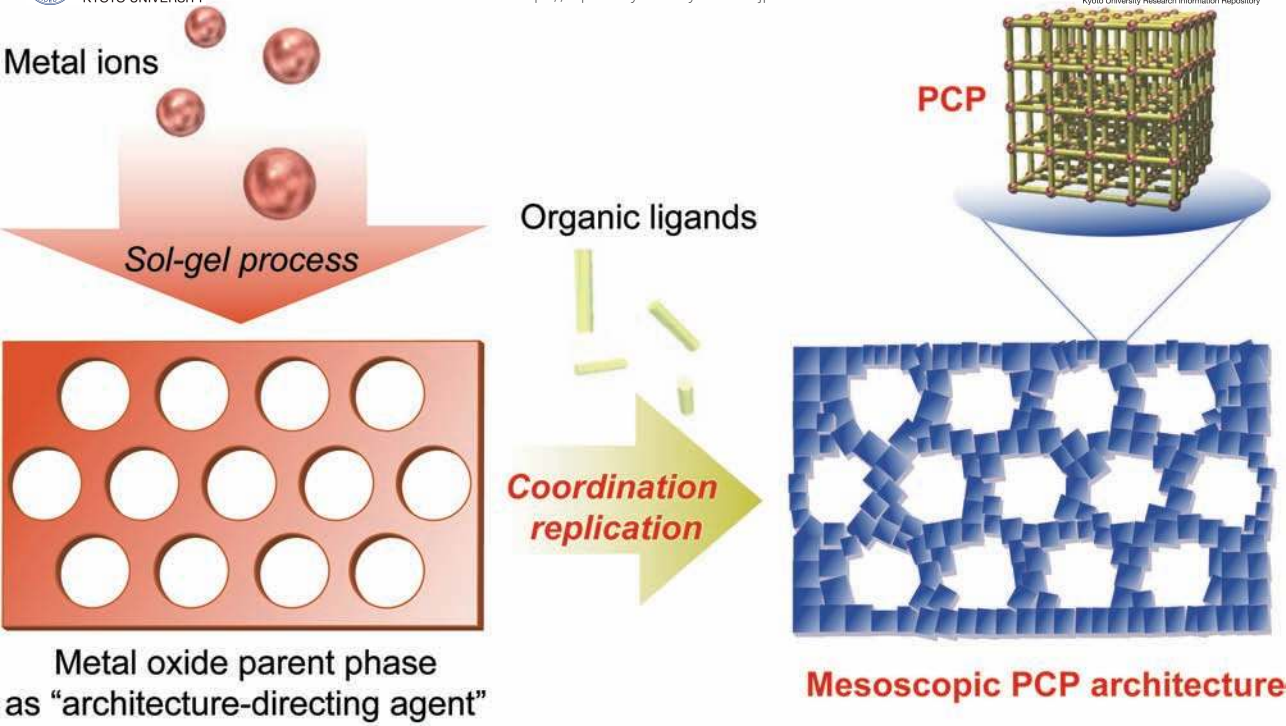

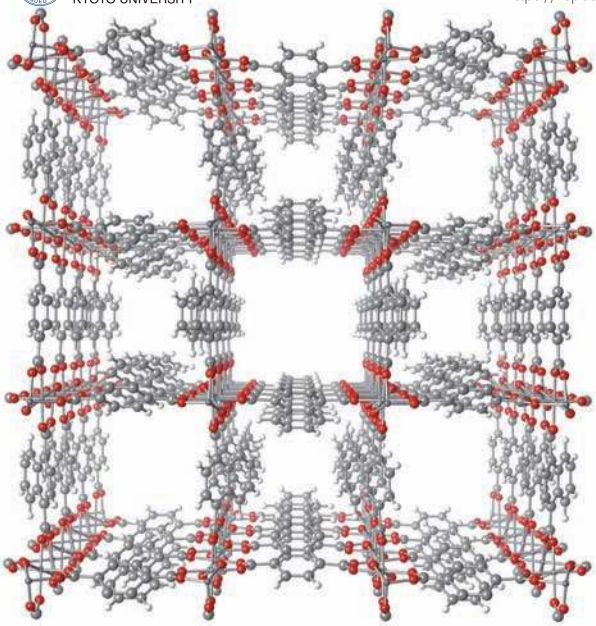

b

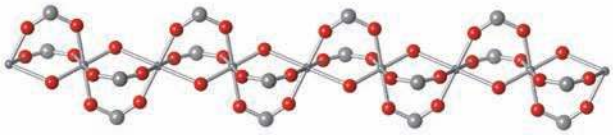

c

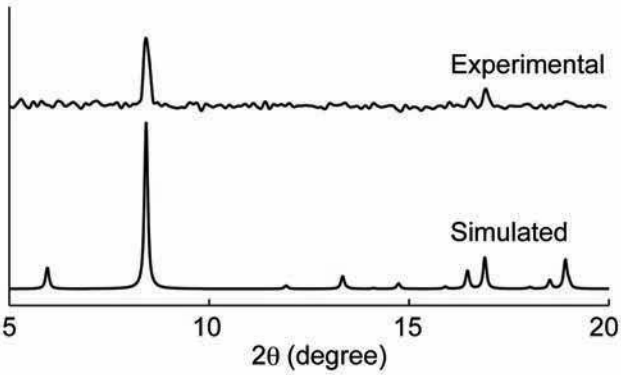

d

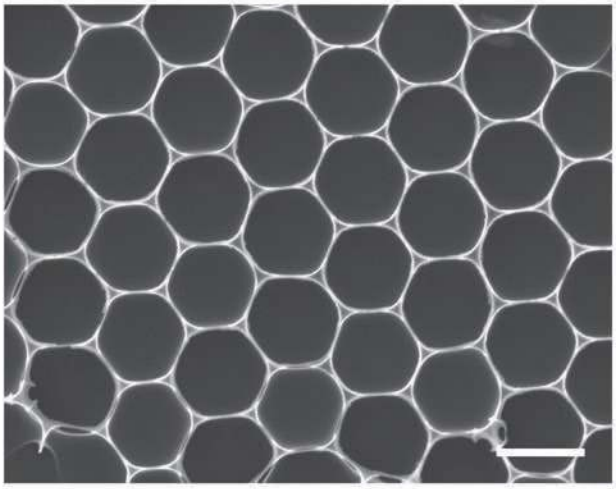

e

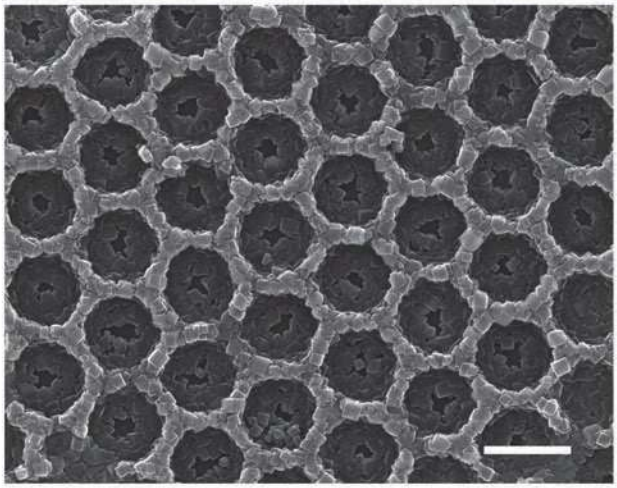

f

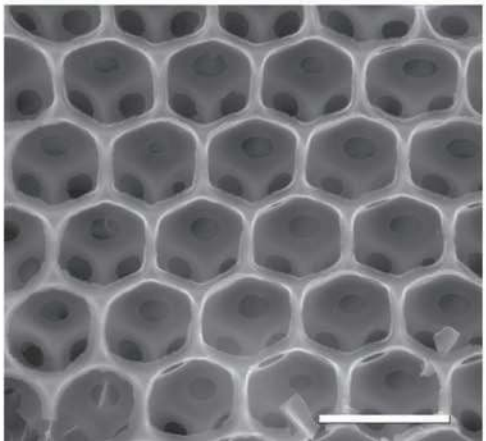

g

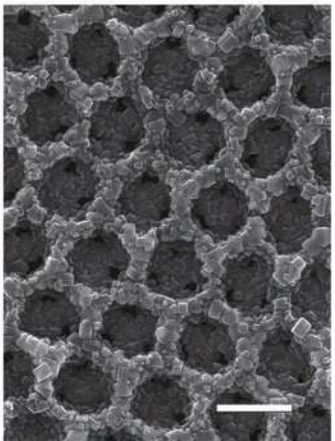

h

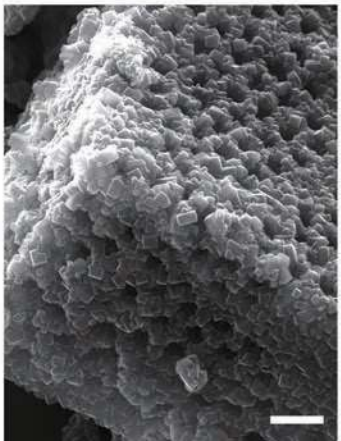

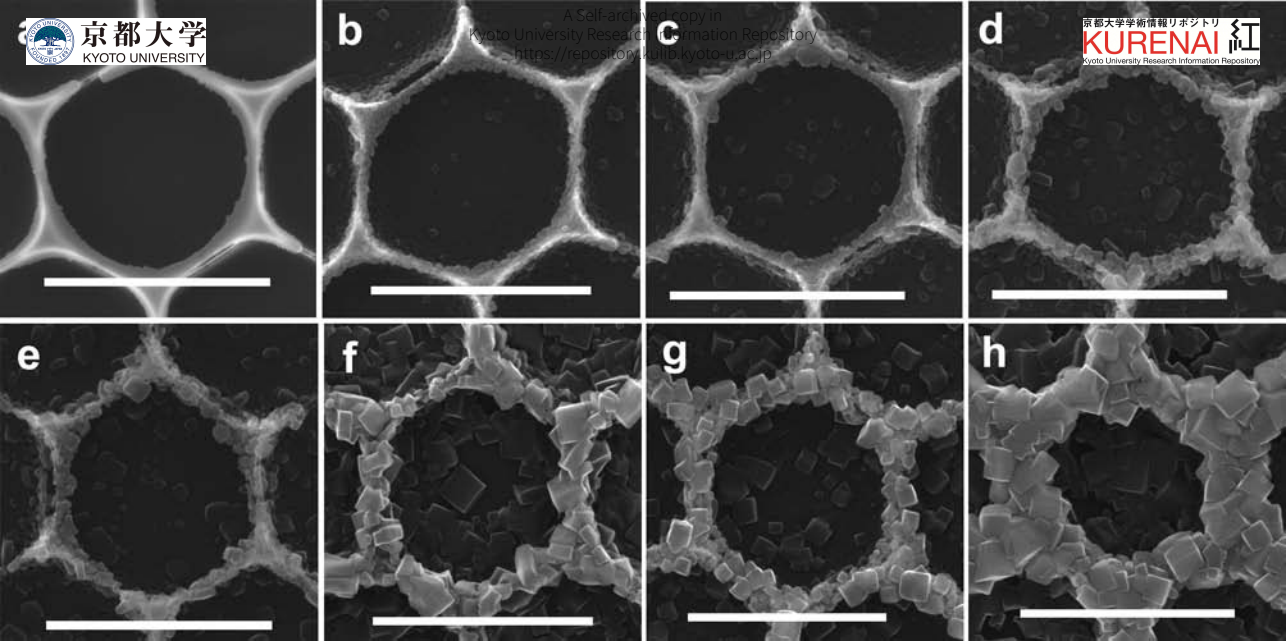

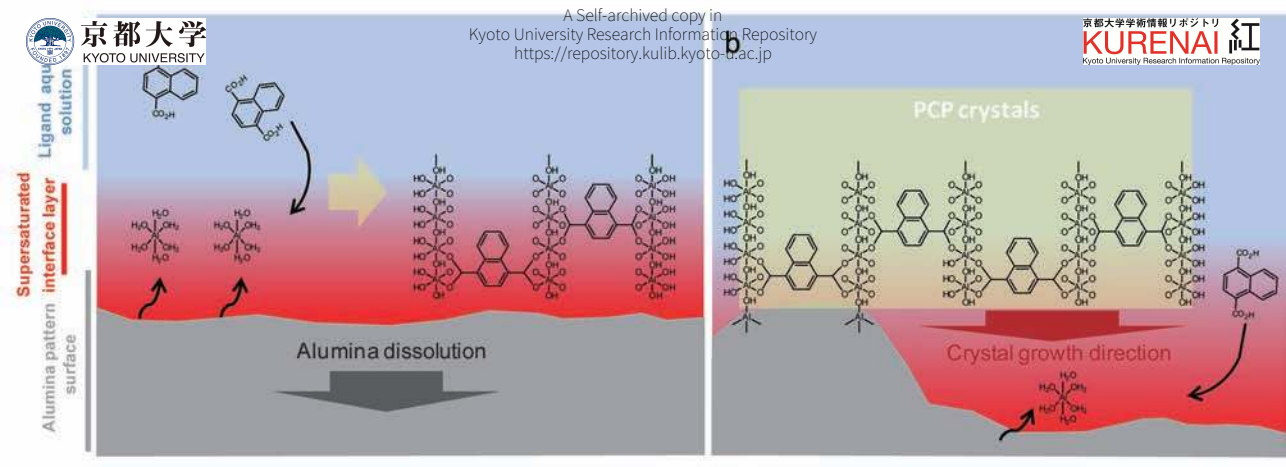

a

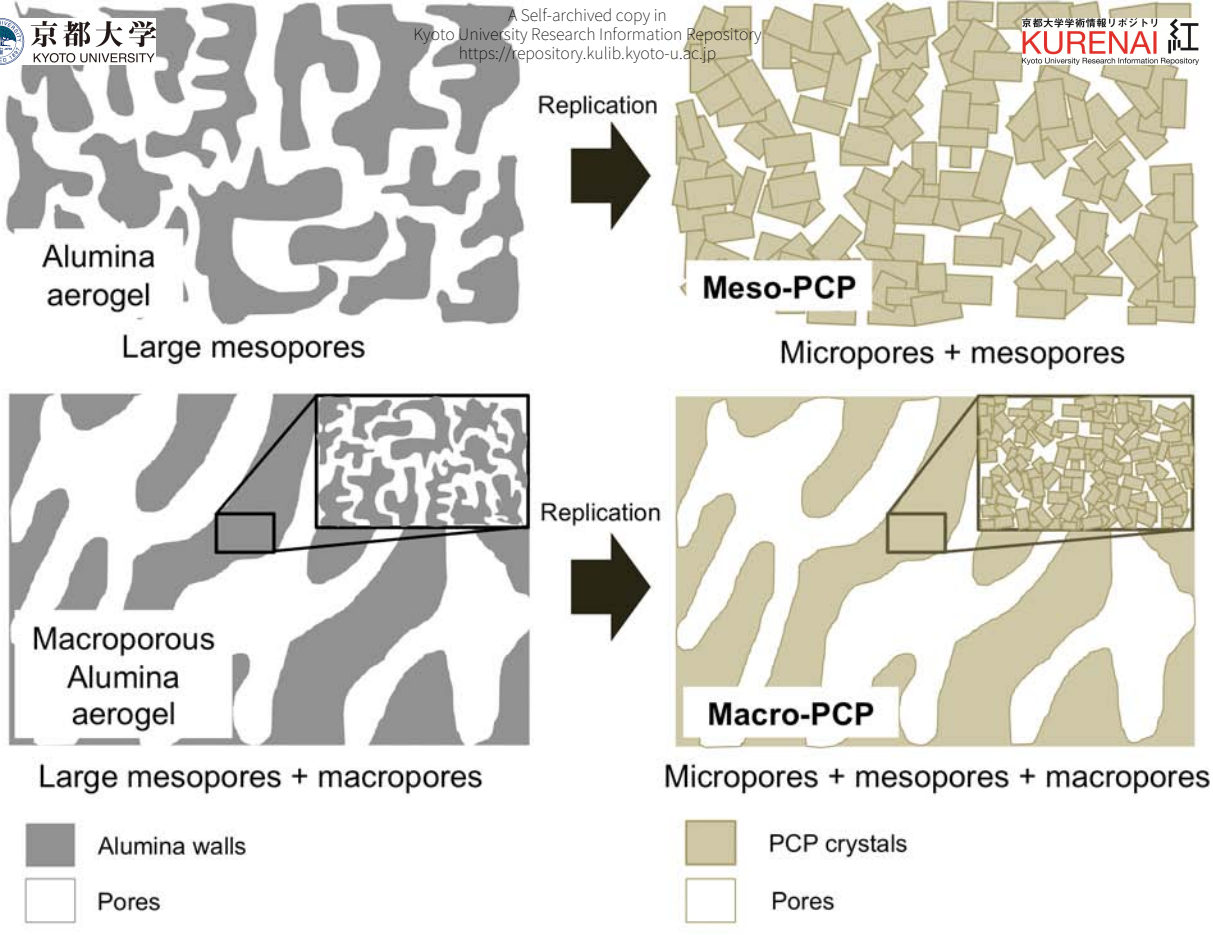

b

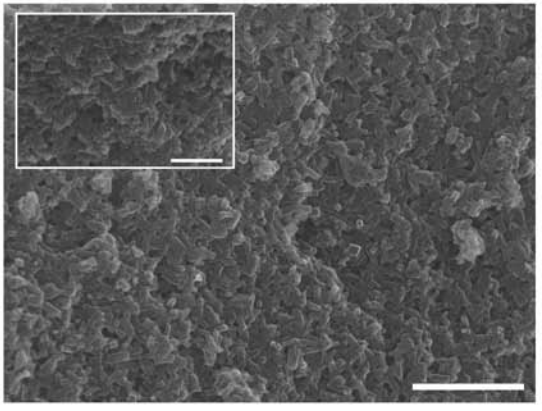

c